Solid State Ionics 262 (2014) 165–169

Contents lists available at ScienceDirect

Solid State Ionics

journal homepage: www.elsevier.com/locate/ssi

Fabrication of thin-film lithium batteries with 5-V-class $LiCoMnO_4$ cathodes

Naoaki Kuwata *, Shota Kudo, Yasutaka Matsuda, Junichi Kawamura

Institute of Multidisciplinary Research for Advanced Materials, Tohoku University, Katahira 2-1-1, Aoba-ku, Sendai 980-8577, Japan

ARTICLE INFO

Article history:
Received 17 May 2013
Received in revised form 20 September 2013
Accepted 28 September 2013
Available online 21 October 2013

Keywords:
All-solid-state battery
Thin film
Pulsed laser deposition
Spinel structure
Cyclic voltammetry

ABSTRACT

All-solid-state thin-film batteries with a 5-V-class cathode material ($LiCoMnO_4$) were fabricated. $LiCoMnO_4$ thin films were grown by pulsed laser deposition. X-ray diffraction and cyclic voltammetry (CV) were used to characterize the thin films. Effects of deposition parameters on the structure, morphology, and electrochemical properties of the thin films were investigated, particularly the influence of oxygen partial pressure, laser fluence, and substrate temperature. The CV curves of the $LiCoMnO_4$ thin films prepared under optimized conditions exhibited reversible 5-V charge/discharge peaks. Thin-film batteries fabricated with $LiCoMnO_4$ cathodes operated at potentials greater than 5 V, which is among the highest voltages reported for a thin-film battery. The thin-film battery also showed good cycling performance at 5 V, with an initial discharge capacity of 107 mAh/g and a capacity retention of 99.4% after 20 cycles.

1. Introduction

All-solid-state thin-film batteries have attracted attention because of their advantages of low self-discharge, long cycle life, and outstanding safety characteristics compared to those of conventional lithium batteries [1,2]. Amorphous LiPON [3] or Li_3PO_4 films [4] have been used as solid electrolytes in 4-V-class solid-state batteries with $LiCoO_2$ as a cathode and Li as an anode. The electrochemical stability window of these electrolytes was greater than 5 V at room temperature [5,6]. Thus, the fabrication of solid-state thin-film batteries with higher-voltage cathode materials instead of $LiCoO_2$ films is expected.

$LiCoMnO_4$, which was first reported by Kawai et al. [7–9], is a promising high-potential cathode with a spinel structure. The 5-V behavior of this material has been attributed to the $Co^{3+/4+}$ redox couple [10,11]. However, few investigations of $LiCoMnO_4$ have been reported in the literature, probably because of electrolyte decomposition at potentials that exceed the voltage stability window of liquid electrolytes [12]. Although Dokko et al. reported the preparation of $LiCoMnO_4$ thin films by electrostatic spray deposition [13], the literature contains no reports of the physical vapor deposition of $LiCoMnO_4$.

In this study, we report the thin-film growth of a spinel $LiCoMnO_4$ cathode by pulsed laser deposition (PLD). The electrochemical properties of $LiCoMnO_4$ were studied to show a correlation between the capacity in the 5-V region and the oxygen partial pressure. Finally, the electrochemical properties of $Li/Li_3PO_4/LiCoMnO_4$ thin-film batteries were demonstrated.

2. Experimental

2.1. Fabrication and characterization of $LiCoMnO_4$ thin films

Ceramics of $LiCoMnO_4$ were synthesized by a solid-state reaction method according to the procedure described in the literature [7]. Stoichiometric mixtures of Li_2CO_3, CoO, and $MnCO_3$ were ground thoroughly, heated in a muffle furnace at a rate of 100 °C/h, and then sintered in air at 800 °C for 24 h. The mixture was subsequently sintered at 600 °C for 3 days with intermittent regrinding and was finally quenched to room temperature.

A target of $LiCoMnO_4$ with a diameter of 25.4 mm and a thickness of 2 mm was prepared by hydrostatic pressing at 70 MPa followed by sintering at 600 °C for 24 h. The relative density of the obtained target was 70% of the theoretical density of $LiCoMnO_4$ (4.69 g/cm^3) calculated from the lattice parameter of $a = 8.058$ Å determined by X-ray diffraction (XRD).

Thin films of $LiCoMnO_4$ were grown by PLD. The main PLD chamber (PLAD-241-LS, AOV) was combined with a glove box (UN-800L, UNICO) and a thermal evaporation system (VPC-061, ULVAC KIKO). The substrate and target were transferred via a load-lock system under an Ar atmosphere. The main chamber was evacuated to 1×10^{-4} Pa, and then high-purity oxygen gas was introduced. The fourth harmonic of a Nd:YAG laser (GCR-150-10, Spectra-Physics) was used. The laser was scanned with a mirror galvanometer to uniformly ablate the target surface. The thickness of $LiCoMnO_4$ thin films was measured with a

* Corresponding author.
E-mail address: kuwata@tagen.tohoku.ac.jp (N. Kuwata).

0167-2738
http://dx.doi.org/10.1016/j.ssi.2013.09.054

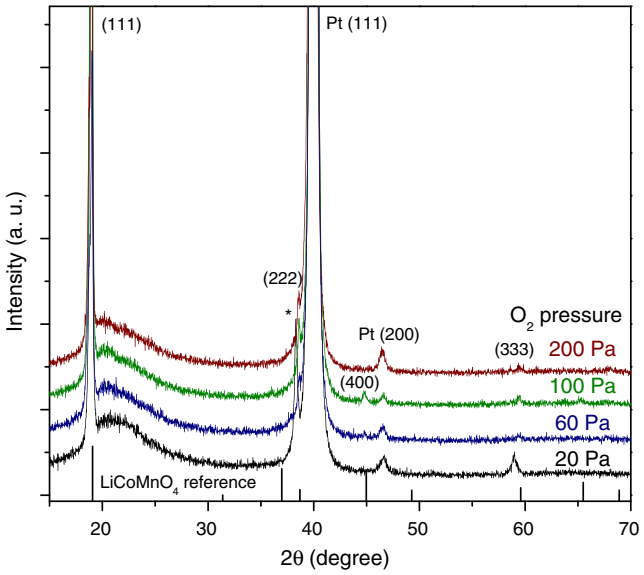

Fig. 1. XRD patterns of $LiCoMnO_4$ thin films deposited on $Pt/Cr/SiO_2$ substrates. The oxygen partial pressure was varied from 20 to 200 Pa. The substrate temperature was 500 °C. The asterisk (*) indicates an impurity phase in the film prepared under 20 Pa.

surface profilometer (SE3000, Kosaka Laboratory). The weight of a film was estimated by subtracting a weight of substrate before deposition from that of the substrate with thin film after deposition using an ultra-microbalance (XP2U, Mettler Toledo). Surface morphology of the thin films was observed using an optical microscope (VK-9710, Keyence) and a scanning electron microscope (FE-SEM, SU6600, Hitachi).

The compositions of the films and powder were analyzed by inductively coupled plasma atomic emission spectroscopy. $LiCoMnO_4$ powder and thin films were dissolved in aqua regia and then diluted in water. The composition of the sintered $LiCoMnO_4$ target was Li:Co:Mn = 1.02:1.01:1, which showed that the target had a stoichiometric composition. The composition of the $LiCoMnO_4$ thin film grown under standard conditions (500 °C, 20 Pa, 2 J/cm^2) was Li:Co:Mn = 0.99:0.98:1, which was also nearly stoichiometric.

An electrochemical cell was assembled with the $LiCoMnO_4$ thin film on a $Pt/Cr/SiO_2$ glass substrate as the positive electrode, Li metal foil as the negative electrode and reference electrode, and 1 mol/L $LiPF_6$ in ethylene carbonate–dimethyl carbonate (EC:DMC, 1:1 volume, Kishida Chemical) as the electrolyte. The area of the $LiCoMnO_4$ film was 0.56 cm^2 for liquid electrolyte. The thicknesses of the films were ca. 150 nm for 20 Pa and ca. 110 nm for 100 Pa, respectively. The thickness of $LiCoMnO_4$ thin film grown at 100 Pa was decreased about 70% of the thickness of a thin film grown at 20 Pa, although the film thickness includes experimental error. The cell components were dried under vacuum at 80 °C for 24 h and then assembled in an Ar-filled glove box. The cell was tested by cyclic voltammetry (CV) in the range of 3.0–5.5 V vs. Li/Li^+ using a scan rate of 0.5 mV/s. The weight of the thin films was measured using an ultra-microbalance for the capacity calculations.

2.2. Fabrication of thin-film batteries

Solid-state thin-film batteries that consisted of $Li/Li_3PO_4/LiCoMnO_4$ thin films on $Pt/Cr/SiO_2$ substrates were constructed. Details of the thin-film battery fabrication are described in our previous reports [14,15]. Since the $LiCoMnO_4$ and Li_3PO_4 thin films were prepared in the same PLD chamber after the target was exchanged, the cathode/electrolyte interface was maintained clean without any impurities. An amorphous Li_3PO_4 electrolyte was deposited by PLD using an ArF excimer laser (COMPex 201, Coherent) [4]. Metallic Li thin films were grown by thermal evaporation. The size of the cathodes was 3 mm × 3 mm. The thicknesses of the films were ca. 150 nm for 20 Pa and ca. 110 nm for 100 Pa, respectively. The anode was 3 mm × 3 mm and several micrometers in thickness. The solid electrolyte was 5 mm × 5 mm and 2–3 μm in thickness. The thin-film batteries were placed inside a vacuum-tight stainless steel cell. Gold wire and silver paste were used to contact between the cell and thin-film batteries electrically. The electrochemical measurements were conducted at 25 °C under vacuum.

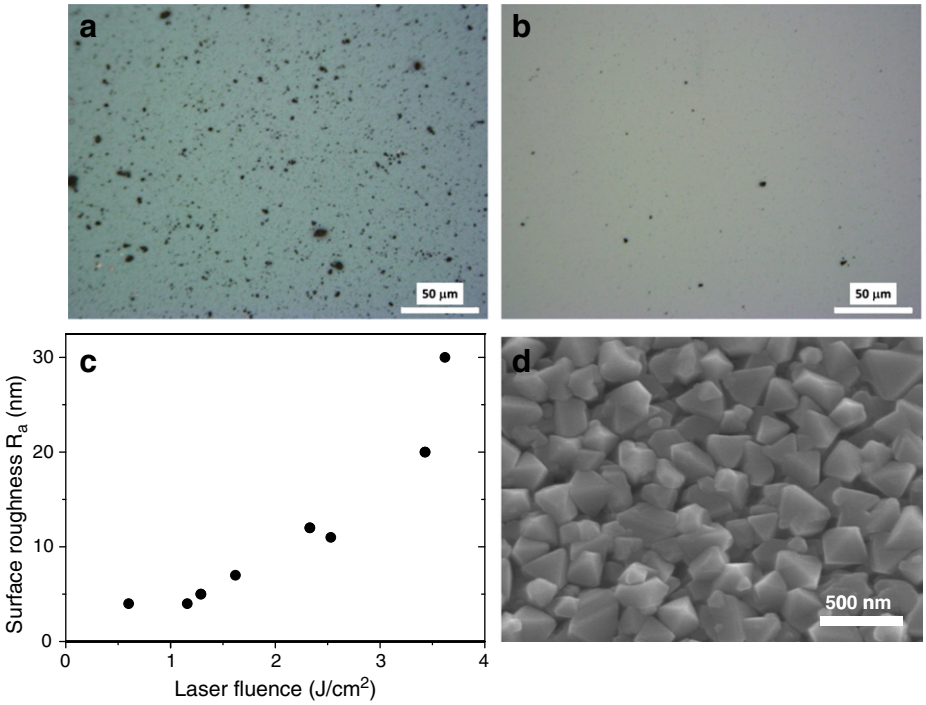

Fig. 2. Optical microscope images of the thin films deposited with laser fluences of (a) 2.3 J/cm and (b) 1.2 J/cm. The surface roughness as a function of the laser fluence is shown in (c). Panel (d) shows a FE-SEM surface view of the $LiCoMnO_4$ film grown at 1.2 J/cm and 100 Pa.

3. Results and discussion

3.1. Structure and morphology of $LiCoMnO_4$ thin films

The quality of the $LiCoMnO_4$ thin film was optimized by the variation of the deposition parameters, including the laser energy density, substrate temperature, and oxygen partial pressure. Fig. 1 shows the XRD patterns of the thin films deposited on $Pt/Cr/SiO_2$ substrates. An X-ray diffractometer (RINT 2100V, Rigaku) equipped with a Cu K_α source was used for the measurements. The observed peaks were attributed to the Bragg reflections of $LiCoMnO_4$. The relative intensities of the Bragg reflections of the films indicate a (111) orientation. The film growth mechanism was strongly influenced by the orientation of the Pt film on the substrate. When the oxygen pressure was decreased, the Bragg reflections shifted to lower angles. This shift is attributed to the lattice expansion of the spinel structure. The lattice parameters were 8.081 Å and 8.138 Å for the films grown under oxygen pressures of 100 Pa and 20 Pa, respectively. The lattice parameter of the bulk material (8.058 Å) was similar to that of film grown under an oxygen pressure of 100 Pa. The transition-metal ions would be reduced at low oxygen pressures, resulting in the formation of oxygen vacancies. The oxygen vacancies formed would diminish the electrostatic attraction between the metal and oxygen atoms; as a consequence, the lattice parameter would increase. In addition, an impurity phase was detected at $2\theta = 38.30°$ in the XRD pattern of the film grown at 20 Pa, as shown in Fig. 1. This peak may be due to the (222) reflection of $LiMn_2O_4$ or the (006) reflection of $LiCoO_2$. The formation of an impurity phase, such as $LiMn_2O_4$, is due to the reduction of Mn^{4+} to Mn^{3+} under a lower oxygen pressure. When the oxygen pressure was increased to greater than 300 Pa, the deposition rate substantially decreased because of the scattering effect of gas molecules. Therefore, we conclude that the optimal condition for oxygen pressure is between 100 and 200 Pa.

Concerning the substrate temperature, we evaluated the XRD patterns of samples prepared with substrate temperatures between 500 °C and 700 °C. For samples prepared at a substrate temperature of 700 °C, the lattice parameter increased because of increased oxygen vacancies. Thus, we used a substrate temperature of 500 °C for subsequent studies.

Surface morphology is an important factor for the fabrication of thin-film batteries. A rough surface frequently causes short circuits (i.e., direct contact between the cathode and anode), because the thickness of the solid electrolyte is only a few micrometers in most cases. The surface morphology and roughness of samples prepared under various growth conditions were investigated by laser microscopy. As a result, we determined that the laser fluence had the most pronounced effect on morphology. The substrate temperature, oxygen pressure, and film thickness minimally affected the surface morphology.

Fig. 2(a)–(c) shows the relationship between the laser fluence and the surface roughness of the $LiCoMnO_4$ thin films. The microscope images clearly show that lower laser fluence improves surface homogeneity. Black particles observed in the microscope images were randomly shaped $LiCoMnO_4$ particles ejected from the target during ablation (exfoliation) [16]. Owing to the low relative density (70%) of the target, if the laser fluence is much higher than the ablation threshold, the shock of ablation would damage the target surface to form micron-sized particles. From these results, we conclude that the optimum laser fluence is less than 1 J/cm^2. Fig. 2(d) shows a SEM surface view of the $LiCoMnO_4$ thin film grown at 1.2 J/cm and 100 Pa. The $LiCoMnO_4$ films consist of small triangle or octahedral crystalline grains. The sizes of crystalline grains are around 300 nm. The triangle shape of grains is caused from the (111) orientation of the cubic spinel structure of $LiCoMnO_4$.

3.2. Electrochemical tests of $LiCoMnO_4$ thin films

The electrochemical properties of the $LiCoMnO_4$ thin films were evaluated using a liquid electrolyte and a beaker cell. Film deposition was performed under the following conditions: a substrate temperature of 500 °C, a laser fluence of 1.0 J/cm^2, and a deposition time of 2 h; the oxygen pressure was varied from 20 Pa to 100 Pa.

Fig. 3 shows CV curves of the $LiCoMnO_4$ films deposited on $Pt/Cr/SiO_2$. Reversible peaks were observed at 3.9, 4.9, and 5.1 V, which indicate the extraction/insertion of Li from/into the thin films. The peak at 3.9 V is associated with the $Mn^{3+/4+}$ redox couple in the spinel structure [9,11]. Dokko et al. reported that the $Mn^{3+/4+}$ redox peak occurs at 4.0 V in the case of the $LiCo_xMn_{2-x}O_4$ spinel structure when x is less than 1 [13]. The large peak at 3.9 V in the CV curve of the sample prepared under an oxygen pressure of 20 Pa indicates that some Mn^{3+} remains in the structure. Moreover, Mn^{3+} will also be produced by the introduction of oxygen defects. As shown in Fig. 3(b), higher oxygen pressures resulted in decreased intensities of the 3.9-V peak until the pressure increased up to 100 Pa. Another possibility for the 3.9-V peak is the $Co^{3+/4+}$ redox couple of layered $LiCoO_2$, which was suggested as an impurity phase by XRD analysis.

The peaks at 4.8 and 5.1 V are associated with the $Co^{3+/4+}$ redox couple in the spinel structure [9–11]. The two peaks are easily recognized in the 5-V region of the cyclic voltammograms of the PLD-grown thin films. These peaks have also been observed in the cyclic voltammograms of a $LiCoMnO_4$ film prepared by electrostatic spray deposition [13]. By analogy with spinel $LiMn_2O_4$, these double peaks are associated with the order–disorder phase transition of Li ions in the spinel structure, where Li ions in the 8a site could form the ordered phase in Li_xCoMnO_4 at $x = 0.5$ [17]. Because PLD-grown thin films are generally highly crystalline [18], the ordered phase and double peaks are thought to appear more clearly. At potentials greater than 5 V, an upward slope was observed in the CV curve shown in Fig. 3. This upward

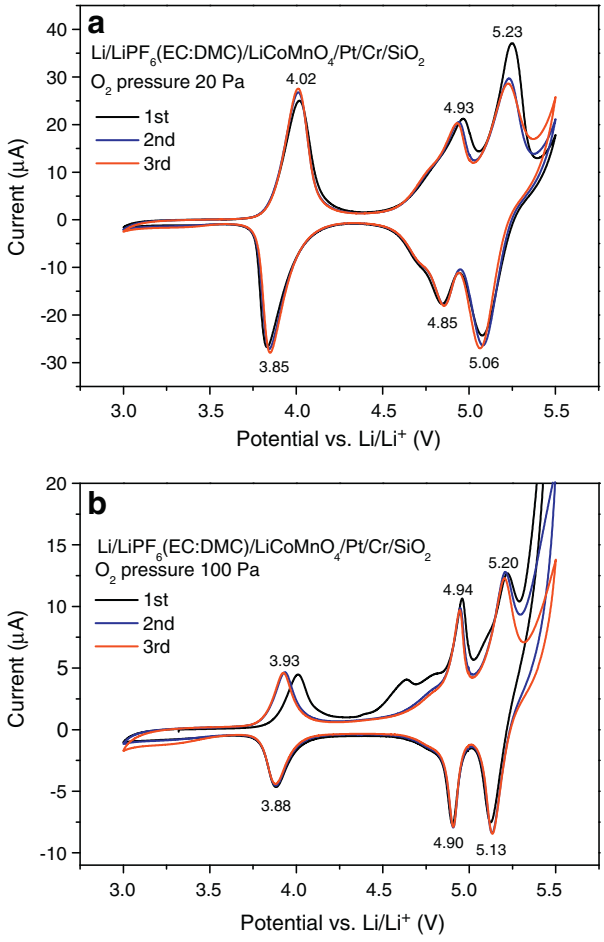

Fig. 3. CV curves of $LiCoMnO_4$ films with 1 mol/L $LiPF_6$ in EC:DMC as the electrolyte. The $LiCoMnO_4$ films were deposited under (a) 20 Pa and (b) 100 Pa of O_2. The sweep rate was 0.5 mV/s.

slope is due to the decomposition of the liquid electrolyte; thus, an estimation of the capacity was difficult.

3.3. Thin-film batteries using $LiCoMnO_4$ thin films

Although the conditions were optimized, the $LiCoMnO_4$ films still contained a small number of exfoliated particles. The presence of these particles makes it difficult to fabricate batteries without short circuits. However, after numerous attempts, we finally succeeded in assembling thin-film batteries with $LiCoMnO_4$ cathodes.

The electrochemical properties of the thin-film batteries are shown in Figs. 4 and 5. The $LiCoMnO_4$ films represented in Figs. 4 and 5 were deposited at oxygen pressures of 20 Pa and 100 Pa, respectively. The CV curves of the thin-film batteries showed charge/discharge peaks at 3.9, 4.8, and 5.2 V, which are attributed to $Mn^{3+/4+}$ and $Co^{3+/4+}$ redox couples in the spinel structure. The operating potential over 5 V is among the highest operating voltages yet reported [19]. For a comparison, thin-film batteries with a $LiCoPO_4$ cathode have been shown to operate at 4.8 V [19].

As shown in Fig. 4(b), the capacity during the first discharge cycle was 107 mAh/g, which is 76% of the theoretical discharge capacity (145 mAh/g) of $LiCoMnO_4$. The authors of previous studies have reported capacities of approximately 90–110 mAh/g [7,12]. The $LiCoMnO_4$ films with a solid electrolyte appears to show much smaller current peaks in CVs (less than 1/10), in contrast to the films with a liquid electrolyte (e. g. Figs. 3(a) and 4(a)). The difference is due to the area and thickness; (1) the area of the films for liquid electrolyte is 0.56 cm^2 while for solid electrolyte is 0.09 cm^2; and (2) the thickness of the films for liquid electrolyte was ca. 150 nm while for solid electrolyte was ca. 100 nm. Thus the capacity of the $LiCoMnO_4$ films with the liquid electrolyte is as large as 10 times of that with the solid electrolyte. The thin-film battery maintained 99.4% of its discharge capacity between the second and twentieth cycles. However, the efficiency of charge and discharge was 95%. The irreversible capacity was possibly due to the side reactions of the Li_3PO_4 electrolyte at potentials greater than 5 V. Although it is suppressed, a very small decomposition current has been observed at potentials greater than 4.8 V [14]. The development of more stable thin-film solid electrolytes is desired in future studies.

As shown in Fig. 5(a), the area under the curves in the 5-V region was increased for a $LiCoMnO_4$ film grown under an oxygen pressure of 100 Pa, similar to the case of the liquid batteries shown in Fig. 3(a). The capacity was 23% for the 4-V region and 73% for the 5-V region during the second cycle shown in Fig. 5(a). Because the initial cycle showed unusual CV behavior, the figure shows only the results obtained after second cycles. Current peaks at the 5-V region showed increased polarization after 20 cycles, while those around 4 V are more stable. The difference in the polarization at 5-V and 4-V regions could be due to different grains in the thin film. The $LiCoMnO_4$ films consist of small crystalline grains as confirmed by FE-SEM shown in Fig. 2(d). The $LiCoMnO_4$ particles containing Mn^{3+} show the peaks around 4 V, while the particles containing Mn^{4+} show the peaks around 5 V. Another possibility is impurities; such as $LiMn_2O_4$ and $LiCoO_2$. Micro Raman spectroscopy suggests the existence of $LiCoO_2$ impurity even in the $LiCoMnO_4$ films grown at 100 Pa (results are not shown). The cycle performance of $LiCoO_2$ at 4-V region is quite stable. Thus the interface resistance of 4-V does not change after cycling, while the interface resistance of 5-V region gradually increases. The thin-film battery with a $LiCoMnO_4$

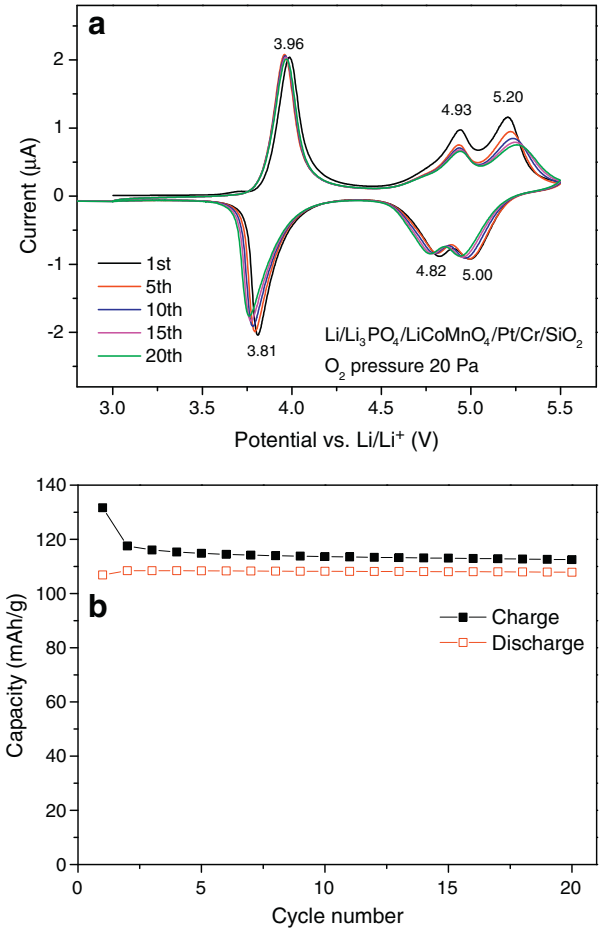

Fig. 4. CV curves (a) and capacities (b) of a $Li/Li_3PO_4/LiCoMnO_4$ thin-film battery. The $LiCoMnO_4$ film was deposited under 20 Pa of O_2. The sweep rate was 0.5 mV/s.

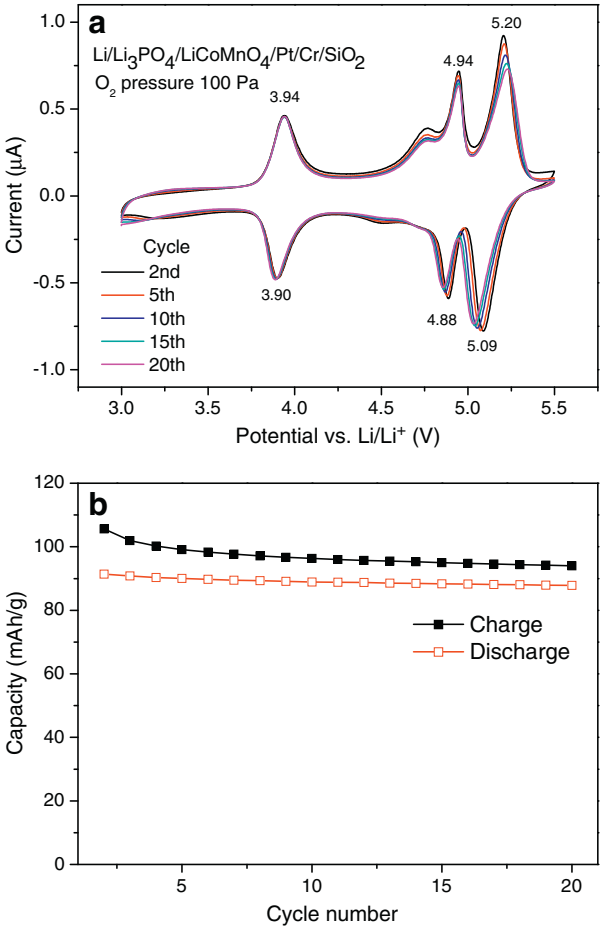

Fig. 5. CV curves (a) and capacities (b) of a $Li/Li_3PO_4/LiCoMnO_4$ thin-film battery. The $LiCoMnO_4$ film was deposited under 100 Pa of O_2. The sweep rate was 0.5 mV/s. Because the initial cycle showed unusual CV behavior, the figure shows only the results obtained after second cycle.

cathode (100 Pa) also showed good cycling performance at 5 V as shown in Fig. 5(b). It retained 95% of its capacity after 20 cycles.

4. Conclusion

$LiCoMnO_4$ thin films for use in thin-film batteries were grown by PLD. The optimized conditions for PLD were a laser energy density of 1 J/cm^2, a substrate temperature of 500 °C, and an oxygen partial pressure of 100 Pa. The resulting $LiCoMnO_4$ films showed a (111) orientation on the Pt/Cr/SiO_2 substrates. Electrochemical properties were strongly affected by the oxygen pressure. The peak areas in the 5-V region of the cyclic voltammograms increased in the case of films grown at 100 Pa. Thin-film batteries fabricated using the prepared $LiCoMnO_4$ cathodes were operated at potentials greater than 5 V, which is among the highest-voltage thin-film batteries yet reported. Excellent cycle performance of the all-solid-state thin-film batteries was demonstrated.

Acknowledgments

This study was supported by JSPS KAKENHI, Grant Number 24550206. This study was also partly supported by the NEDO RISING Battery Project.

References

[1] J.F.M. Oudenhoven, L. Baggetto, P.H.L. Notten, Adv. Energy Mater. 1 (2011) 10–33.
[2] A. Patil, V. Patil, D.W. Shin, J.-W. Choi, D.-S. Paik, S.-J. Yoon, Mater. Res. Bull. 43 (2008) 1913–1942.
[3] X. Yu, J.B. Bates, G.E. Jellison Jr., F.X. Hart, J. Electrochem. Soc. 144 (1997) 524.
[4] N. Kuwata, N. Iwagami, J. Kawamura, Solid State Ionics 180 (2009) 644.
[5] J. Bates, N.J. Dudney, B.J. Neudecker, F.X. Hart, H.P. Jun, S.A. Hackney, J. Electrochem. Soc. 147 (2000) 59.
[6] Y. Iriyama, T. Kako, C. Yada, T. Abe, Z. Ogumi, Solid State Ionics 176 (2005) 2371.
[7] H. Kawai, M. Nagata, H. Kageyama, H. Tukamoto, A.R. West, Electrochem. Solid State Lett. 1 (1998) 212.
[8] H. Kawai, M. Nagata, H. Kageyama, H. Tukamoto, A.R. West, J. Mater. Chem. 8 (1998) 837.
[9] H. Kawai, M. Nagata, H. Kageyama, H. Tukamoto, A.R. West, Electrochim. Acta 45 (1999) 315.
[10] D. Pasero, S. de Souza, N. Reeves, A.R. West, J. Mater. Chem. 15 (2005) 4435–4440.
[11] P. Aitchison, B. Ammundsen, D.J. Jones, G. Burns, Jacques Rozière, J. Mater. Chem. 9 (1999) 3125–3130.
[12] X. Huang, M. Lin, Q. Tong, X. Li, Y. Ruan, Y. Yang, J. Power Sources 202 (2012) 352–356.
[13] K. Dokko, N. Anzue, M. Mohamedi, T. Itoh, I. Uchida, Electrochem. Commun. 6 (2004) 384–388.
[14] N. Kuwata, N. Iwagami, Y. Tanji, Y. Matsuda, J. Kawamura, J. Electrochem. Soc. 157 (2010) A521.
[15] N. Kuwata, J. Kawamura, K. Toribami, T. Hattori, N. Sata, Electrochem. Commun. 6 (2004) 417.
[16] D.B. Chrisey, G.K. Hubler, Pulsed Laser Deposition of Thin Films, Wiley, New York, 1994.
[17] Y. Gao, J.N. Reimers, J.R. Dahn, Phys. Rev. B 54 (1996) 3878.
[18] T. Ohnishi, B.T. Hang, X. Xu, M. Osada, K. Takada, J. Mater. Res. 25 (2010) 1886.
[19] W.C. West, J.F. Whitacre, B.V. Ratnakumar, J. Electrochem. Soc. 150 (2003) A1660–A1666.